analytical chemistry

pubs.acs.org/ac Article

Enhancing Extracellular Vesicle Detection *via* Cotargeting Tetraspanin Biomarkers

Jesus M. Lopez Baltazar, Wenchao Gu, and Qiuming Yu*

Cite This: *Anal. Chem.* 2024, 96, 16406−16414 Read Online

ACCESS | Metrics & More | Article Recommendations | Supporting Information

ABSTRACT: Extracellular vesicles (EVs) are emerging as key diagnostic biomarkers due to their widespread presence in body fluids and the proteins on their surfaces, which reflect the identity and condition of their parent cells. Research has focused on detecting EVs with biosensors that target individual transmembrane proteins (TMPs) like tetraspanins. However, due to TMP heterogeneity and the formation of tetraspanin-enriched microdomains (TEMs), cotargeting multiple TMPs is a promising strategy for enhancing EV detection. In this work, we introduce a dual-antibody surface functionalization approach using surface plasmon resonance (SPR) biosensors to cotarget tetraspanins on EVs derived from mouse macrophages. The expression of EV tetraspanin markers followed the trend of CD9 > CD63 > CD81, which was consistent with the EV detection targeting their nontetraspanin partners, exhibiting LFA-1 > ICAM-1 > VCAM-1, and suggesting a differential role of tetraspanins with their associated TMPs. Cotargeting EV tetraspanins *via* CD81/CD63, CD81/CD9, and CD63/CD9 dual monoclonal antibody surfaces resulted in higher EV detection compared to predictions based on binding with two monoclonal antibodies against tetraspanins without cotargeting. Furthermore, the optimization of dual monoclonal antibody surface ratios to improve cotargeting effect yielded a statistically significant enhancement in the sensitivity of EV detection. These findings underscore the importance of TEMs in designing EV-based biosensing platforms to achieve optimized sensitivity in EV detection.

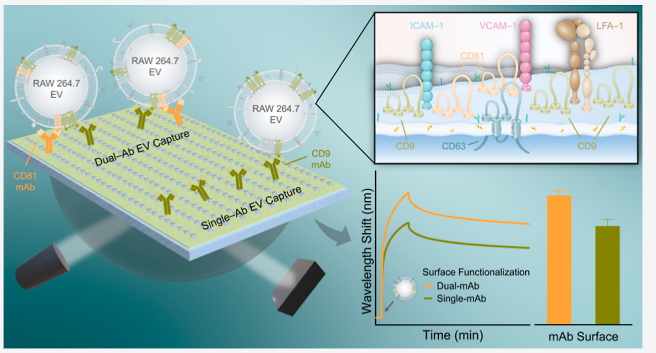

INTRODUCTION

Extracellular vesicles (EVs) are membrane-enclosed particles secreted by all cells.[1−10] EVs are key in intercellular communication processes,[11] waste management, coagulation, and cell homeostasis.[12] When Raposo *et al.* established that EVs were biologically functional,[13] a new field unleashed focused on the fundamental understanding, characterization, and application of EVs as noninvasive disease diagnostic and therapeutic markers.[10,14] Exosomes comprise the most abundant EV subset ranging in size between 30 and 150 nm.[15−18] Exosomal markers are inherited from the multivesicular bodies (MVBs) in the endosomal region of their parent cells,[19] making them valuable biomarker carriers. Specifically, exosomes derived from morbid cells often up- or down-regulate specific transmembrane protein (TMP) biomarkers, contributing to disease progression and resistance to therapy.[20,21] These characteristics make EVs a promising target for diagnostic applications using biosensing technologies.

Tetraspanins comprise large subsets of TMPs, and they are often considered as "molecular facilitators" being involved in cellular proliferation, mobility, and activation.[22,23] CD81, CD63, and CD9 are tetraspanins commonly recognized as universal markers on the surface of EVs.[24,25] In macrophages, CD81 and CD9 prevent the fusion of cells and hinder osteoclastogenesis whereas CD63 is highly expressed on the neotissue generated by intrafibrillarly mineralized collagen.[26−28] Tetraspanins form lateral associations with each other and with multiple partner proteins, creating structures known as tetraspanin-enriched microdomains (TEMs).[29−32] These domains typically span an area of 200−400 nm^2 on the plasma membrane.[30] While the majority of interaction mechanisms within TEMs remain poorly understood, studies have highlighted their involvement in cell-to-cell interactions and in cell-fusion events.[31,32] Primary associations within TEMs are between tetraspanins and nontetraspanin molecules and proteins where associations depend on the cell type.[31] To illustrate, reports have demonstrated a direct association between EV tetraspanins and macrophage TMP partners. Reyes *et al.* used confocal microscopy co-localization and co-immunoprecipitation to report the association of CD9 with the

Received: August 2, 2024
Revised: September 25, 2024
Accepted: September 27, 2024
Published: October 3, 2024

https://doi.org/10.1021/acs.analchem.4c04086
Anal. Chem. 2024, 96, 16406−16414

β2 integrin LFA-1 in T and B monocytic cells.[33] Some findings have shown that upregulation of CD81 in the endothelium of early atherosclerosis lesions increased the clustering of endothelial adhesion molecules ICAM-1 and VCAM-1.[34,35] Furthermore, multiple tetraspanins like CD81 and CD9 have been associated with monocyte-like TMPs such as ICAM-1.[34] Tetraspanin−tetraspanin associations are referred to as secondary interactions.[31] These interactions are not stoichiometric, and it is unclear if all tetraspanins associate with each other in a given cell line.[36] Lastly, tertiary interactions describe the indirect associations of tetraspanins with additional proteins, facilitating membrane lateral organization and intracellular signaling.[31] The formation of TEMs and the heterogeneity of TMPs offer exciting opportunities to enhance EV detection with biosensors through the cotargeting of multiple TMPs.

State-of-the-art biosensing technologies for EV detection target individual tetraspanins with minimal consideration for TEMs.[2,37,38] Among these, labeled-based techniques, such as Western Blot, enzyme-linked immunosorbent assay (ELISA), and flow cytometry,[39−41] pose challenges in terms of detection limits, cost, and immunoassay execution time. Surface plasmon resonance (SPR) biosensors for EV detection have stood out in the past decade due to label-free, real-time, and cost-effective monitoring,[42−56] and they have been applied in the screening, diagnosis and prognosis of Alzheimer's disease and several cancer subtypes including breast, liver, and ovarian.[57,58] Many studies have established the successful capture of EVs *via* CD9, CD63, and CD81.[44,50,51] A common feature of these studies is the use of a single antibody type for targeting tetraspanins. Interestingly, only one work by Wang *et al.* has implemented a CD9/CD81 dual-antibody approach for EV capture using SPR biosensors to profile CD20+ EVs from transfected Expi293 cells.[43] Their work reported binding affinities in ranges of 0.3−7.4 nM and 0.2−12.3 nM of CD20+ EVs with Rituximab and Obinutuzumab, respectively. However, to the best of our knowledge, no work has thoroughly elucidated EV capture enhancement using dual-Ab over single-Ab functionalization strategies using SPR biosensors.

Here, we present a dual-Ab surface functionalization strategy to enhance EV detection with SPR biosensors. Specifically, we co-target tetraspanins CD9, CD63, and CD81 on EVs derived from RAW 264.7 cells. We first determined the expression levels of these tetraspanins on EVs using sandwich assays with SPR biosensors and a comparative double sandwich ELISA. We then investigated EV detection by targeting nontetraspanin TMPs LFA-1, ICAM-1, and VCAM-1, which are associated with TEMs, specifically CD9 and CD81, and correlated these results with the expression levels of their tetraspanin partners. Finally, we performed EV co-capture using a dual-Ab functionalization approach with monoclonal Ab (mAb) against CD81, CD63, and CD9 at varying ratios of 3:1, 1:1, and 1:3. We assessed the statistical significance of EV detection enhancement for each dual-mAb combination and compared it to the single-Ab methodology. This work advances our understanding of EV detection with SPR biosensors considering TEMs, which is key to the development of sensing technologies that can optimally use EV samples for diagnostic applications.

EXPERIMENTAL SECTION

Single- and Dual-mAb Functionalization for EV Detection Using SPR Biosensor. Cell culture, EV isolation, and size/concentration characterization using nanoparticle tracking analysis (NTA) were performed according to the protocol described previously.[59] A home-built SPR biosensor was used and all SPR chips were coated with mixed self-assembled monolayers (SAMs) with OEG_4OH and OEG_6COOH at a molar ratio of 9:1 in solution.[59] For the EV detections with the single-mAb functionalization, immobilized CD9, CD63, and CD81 mAbs with ∼40% surface coverage were used to capture RAW 264.7 derived EVs at a concentration of 2.0×10^{10} EVs/mL. The detection steps were performed for 9 min at 30 μL/min, followed by a washing step with PBS (1×) for 40 min at 20 μL/min. The EV detection with the dual-mAb functionalization was conducted analogously at a fixed EV concentration of 2.0×10^{10} EVs/mL onto the surfaces functionalized with CD81/CD63, CD81/CD9, and CD63/CD9 mAbs at ratios of 1:3, 1:1, and 3:1, respectively, with a total of ∼40% surface coverage. UP BSA was used as a reference surface at the same surface coverage as mAbs.

SPR Sandwich Assays. Sandwich assays were performed by flowing three mAbs in sequence over the SPR sensing surfaces captured EVs by CD9, CD63, and CD81 mAbs, respectively. For example, for EVs captured with CD9 mAbs, after 60 min of washing captured EVs with PBS (1×), CD9, CD63, and CD81 mAbs were flown in sequence at a concentration of 20 μg/mL for 7 min followed by 10 min of PBS (1×) wash in between sequential exposure at a flow rate of 20 μL/min. For EVs captured with CD63 and CD81, respectively, a similar sandwich assay was applied.

Immunocapture-Based Double-Sandwich ELISA for EV Detection. For the ELISA experiments, mAbs used in SPR experiments were used to capture EVs, which are referred to as "capture mAbs". The mAbs used in the sandwich assay to profile tetraspanins are referred to as "detection mAbs", and they are distinctly denoted with an apostrophe (*e.g.*, CD9′ mAbs). The detection mAbs are produced in rabbit hosts to ensure compatibility with the secondary HRP Abs. One series of experiments used CD9, CD63, and CD81 mAbs for EV capture, followed by sandwich with rabbit host CD9′ mAbs. Another series of experiments used CD9 mAbs for EV capture, followed by sandwich with CD9′, CD63′, and CD81′ mAbs for tetraspanin detection on EVs. Experimental details are provided in the Supporting Information.

RESULTS AND DISCUSSION

Single-mAb Surface Functionalization and Sandwich Assays for Profiling Tetraspanin Biomarkers on RAW 264.7 EVs. Single CD81, CD63, and CD9-mAb functionalized SPR sensor surfaces were used for RAW 264.7 EV detection (Figure 1A). The isolated EVs showed an average diameter within 50−150 nm (Figure S1), indicating exosomes were dominant in these samples.[15−18] Figure 1B,C show the SPR detection sensorgrams and the corresponding wavelength shifts for the EV detection using CD81, CD63, and CD9 mAbs and the UP BSA reference surfaces. For each measurement, six replicates were performed on different SPR chips shown in Figure S2. The EV detection levels followed the trend CD9 > CD63 > CD81 with measured wavelength shifts of 7.59 ± 0.99, 3.44 ± 0.55, and 2.43 ± 0.34 nm, respectively. Factors contributing to this trend may include the presence of glycans surrounding tetraspanins,[32,36] variations in glycosylation on the extracellular loop of tetraspanins that affect Ab binding,[60] and

https://doi.org/10.1021/acs.analchem.4c04086
Anal. Chem. 2024, 96, 16406−16414

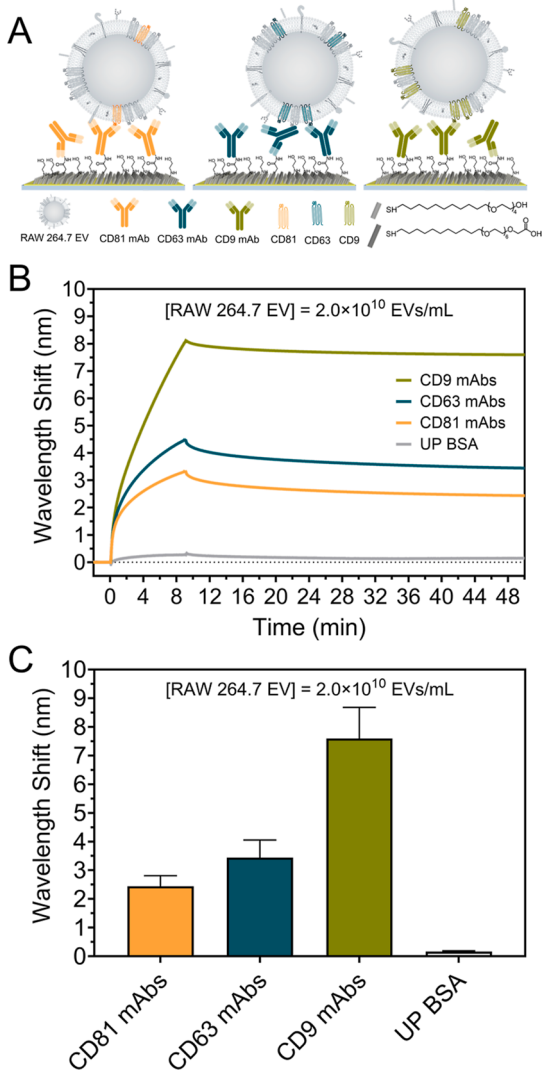

Figure 1. (A) Immunoassay for RAW 264.7 EV detection using CD81, CD63, and CD9-mAb functionalized SPR sensor surfaces. (B) Real-time SPR sensorgrams and (C) wavelength shift of the detection of RAW 264.7 EVs at a concentration of 2.0 × 10^{10} EVs/mL.

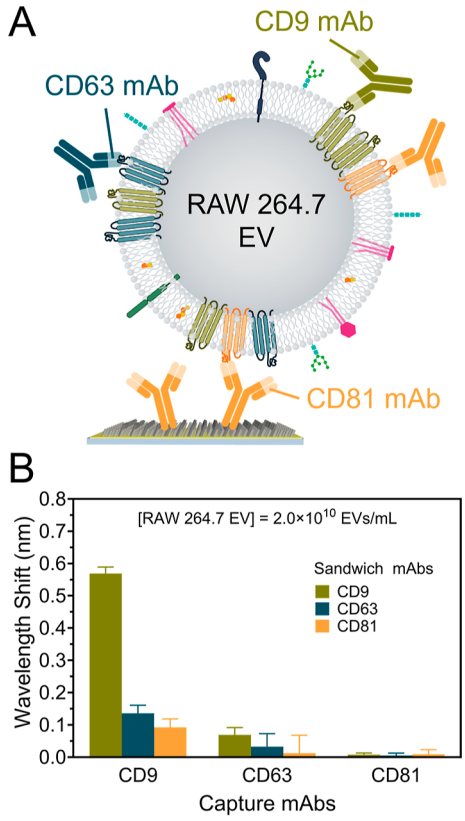

Figure 2. (A) Schematic of an SPR biosensor sandwich assay with CD81, CD63, and CD9 mAbs for the profiling of tetraspanin markers on the surface of RAW 264.7 EVs captured with CD81 mAbs. (B) Wavelength shift of sandwich CD9, CD63, and CD81 mAbs for tetraspanin profiling using the SPR biosensor sandwich assay on RAW 264.7 EVs captured with CD81, CD63, and CD9 mAbs, respectively, at an EV concentration of 2.0 × 10^{10} EVs/mL and mAb concentration of 20 μg/mL.

different expression levels of CD9, CD63, and CD81 tetraspanins on EVs derived from RAW 264.7 cells.

To decouple these effects, we performed sandwich assays to profile tetraspanins on captured EVs. Figure 2A depicts a schematic of the sandwich assay for EVs captured with CD81 mAbs and profiled with CD9, CD63, and CD81 mAbs. The corresponding full and individual SPR sensorgrams are presented in Figure S3. A summary of the binding of mAbs against CD9, CD63, and CD81 tetraspanins on captured EVs is shown in Figure 2B. The increased tetraspanin detection signals observed in the sandwich assay correlate with the number of EVs captured on the SPR chip, following the order: CD9-mAbs > CD63-mAbs > CD81-mAbs. Among the three capture surfaces, CD9 mAbs yield the highest signals in the sandwich assays, followed by CD63 mAbs and CD81 mAbs. For EVs captured with CD9 mAbs, the sandwich wavelength shifts are 0.568 ± 0.016 nm for CD9 mAbs, 0.135 ± 0.020 nm for CD63 mAbs, and 0.092 ± 0.021 nm for CD81 mAbs. When EVs are captured *via* CD63 and CD81 mAbs, the sandwich wavelength shifts of CD9 mAbs decreased dramatically to 0.069 ± 0.018 nm and 0.007 ± 0.003 nm, respectively. This trend was also observed for the sandwich wavelength shifts of CD81 and CD63 mAbs on EVs captured by CD9, CD63 and CD81 mAbs. These results suggest that the expression levels of tetraspanins on EVs are CD9 > CD63 > CD81.

Comparative ELISA Assays for Profiling Tetraspanin Biomarkers on RAW 264.7 EVs. The complex molecular environment on the EV surface influences how effectively Abs bind to tetraspanins. The specific epitope sequences targeted by mAbs can impact their binding efficiency.[61] To investigate this in detail and to verify the tetraspanin profiling results obtained by the SPR sandwich assays, we performed the comparative ELISA assays (Figure 3A,B). We used the same CD81, CD63, and CD9 mAbs to capture EVs on the ELISA plates. For detection in the ELISA sandwich assay, we used mAbs against the same tetraspanins but from different host species, referred to as CD81′, CD63′, and CD9′ mAbs. This approach ensures that differences in epitope recognition across mAbs do not significantly affect the detection results. The detection mAbs were selected to be compatible with the secondary HRP antibodies. Figure 3C presents the ELISA results of EVs at a concentration of 2.1 × 10^{11} EVs/mL captured with CD81, CD63, and CD9 mAbs and sandwiched with CD9′ mAbs. The optical density signal follows the trend: EVs captured with CD9 mAbs > CD63 mAbs > CD81 mAbs, consistent with the SPR results. We further used CD9-mAb

https://doi.org/10.1021/acs.analchem.4c04086
Anal. Chem. 2024, 96, 16406−16414

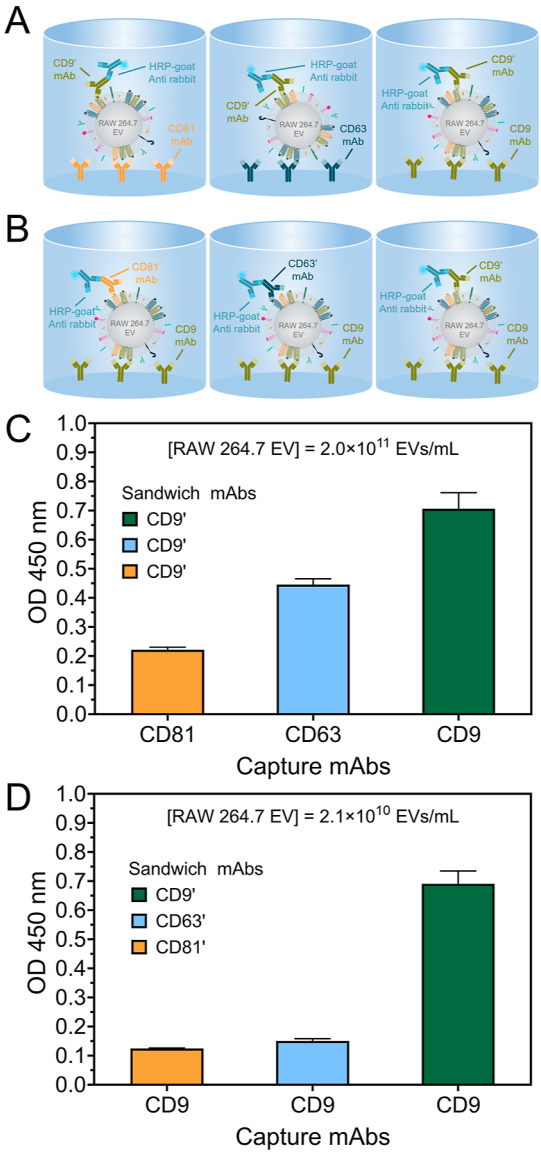

Figure 3. (A) ELISA experiments using CD81, CD63, and CD9 mAbs for RAW 264.7 EV capture, and CD9′ mAbs for detection using a double-sandwich assay. (B) ELISA experiments using CD9 mAbs for RAW 264.7 EV capture, and CD81′, CD63, and CD9′ mAbs for tetraspanin detection using a double-sandwich assay. (C) Optical density (450 nm) from ELISA assay of RAW 264.7 EVs incubated at a concentration of 2.0×10^{11} EVs/mL on CD81, CD63, and CD9 mAbs well plates. The captured EVs were profiled with a sandwich assay using CD9′ mAbs and HRP secondary Abs. (D) Optical density (450 nm) from ELISA assay of RAW 264.7 EVs incubated at a concentration of 2.1×10^{10} EVs/mL on CD9 mAbs well plates. The captured EVs were profiled with a sandwich assay using CD9′, CD63′, and CD81′ mAbs and HRP secondary Abs.

surfaces to capture EVs at 2.1×10^{10} EVs/mL and sandwiched with CD81′, CD63′, and CD9′ mAbs, respectively. Figure 3D shows that with the CD9-mAb surfaces, the sandwich signals follow the trend: CD9′ mAbs > CD63′ mAbs ≈ CD81′ mAbs, aligning with the SPR sandwich assay results. The consistency of these trends across both ELISA and SPR assays, using different primary mAbs, indicates that variations in epitope recognition do not significantly impact the results. Moreover, CD9 tetraspanin is a proteolipid with two glycosylation sites on its EC1 loop,[62] while CD81 tetraspanin is a nonglycerinated protein.[63] CD63 tetraspanin, however, has three N-glycosylation sites on its EC2 loop, which may affect Ab binding.[64,65] Figure S4 provides a schematic of the extracellular loop glycosylation for CD81, CD63, and CD9 tetraspanins. The glycosylation of CD63 tetraspanin may obstruct antibody binding to its EC2 loop, making it challenging to assess its expression level accurately. Given that antibody binding occurs in the EC2 loop, the higher binding observed for CD9 tetraspanin suggests greater CD9 tetraspanin expression compared to CD81 tetraspanin. Furthermore, the pairwise homology percentages in the conserved region of the EC2 loop shows limited similarity among these tetraspanins (Figure S5).[36] For example, CD9 and CD81 tetraspanins share a 20% conserved-EC2 pairwise homology whereas the differences in EV detection are more pronounced with both SPR biosensors and ELISA. CD63 tetraspanin exhibits only 7% and 5% homology with CD81 and CD9 tetraspanins, respectively. The low pairwise homology percentages highlight the distinct nature of these tetraspanins in their extracellular domains. Overall, the consistency in our tetraspanin profiling results suggests that the observed trends for CD9, CD63, and CD81 tetraspanins are directly related to their expression levels on RAW 264.7 EVs.

Detection of Tetraspanin Partner Proteins on RAW 264.7 EVs. Macrophage cells are known to express LFA-1, ICAM-1, and VCAM-1 TMPs.[33−35] Some studies have supported associations of CD9 with LFA-1 and ICAM-1.[33,34] Other reports have correlated CD81 partnership with ICAM-1, and VCAM-1.[34,35] We hypothesized that the expression levels of these nontetraspanin TMPs on EVs might correlate with their tetraspanin partners, as illustrated in Figure 4A. To evaluate this hypothesis, we functionalized the SPR sensor surfaces with LFA-1, ICAM-1, and VCAM-1 mAbs to detect EVs and assess any correlation with their corresponding tetraspanin partners CD9 and CD81. Figure 4B,C display the SPR sensorgrams and wavelength shifts for EV detection using these nontetraspanin TMP mAb-functionalized surfaces. EVs captured with LFA-1 mAbs had the highest wavelength shift of 2.55 ± 0.43 nm compared to 2.23 ± 0.07 nm and 1.90 ± 0.06 nm for EVs captured with ICAM-1 and VCAM-1 mAbs, respectively. These results suggest a direct correlation between the levels of tetraspanin expression on EV and their nontetraspanin TMPs partners. Specifically, CD9 tetraspanin is more highly expressed on RAW 264.7 EVs than CD81 tetraspanin. This may explain the higher EV capture observed with LFA-1 mAbs, reflecting its partnership with CD9 tetraspanin. A similar conclusion is drawn for ICAM-1 and VCAM-1 in their corresponding associations with CD81 tetraspanin. CD9 has been correlated with ICAM-1,[66] which could explain the slightly higher wavelength shift from EV capture compared to VCAM-1. Although the wavelength shifts did not show statistically significant differences in average values and standard deviations, this may be due to variability in experimental replicates. Further experimental repetitions could provide more precise statistical significance. These findings reinforce the trends observed for CD9 and CD81 tetraspanins on EVs, as seen in both SPR and ELISA results.

Moreover, tetraspanin−nontetraspanin partner associations are primary interactions in TEMs.[67] A single tetraspanin molecule can form distinct associations with nontetraspanin TMPs depending on the cell line. In the context of cancer, many TMPs are upregulated or downregulated on the EV surface, depending on the disease type and stage. Therefore,

https://doi.org/10.1021/acs.analchem.4c04086
Anal. Chem. 2024, 96, 16406−16414

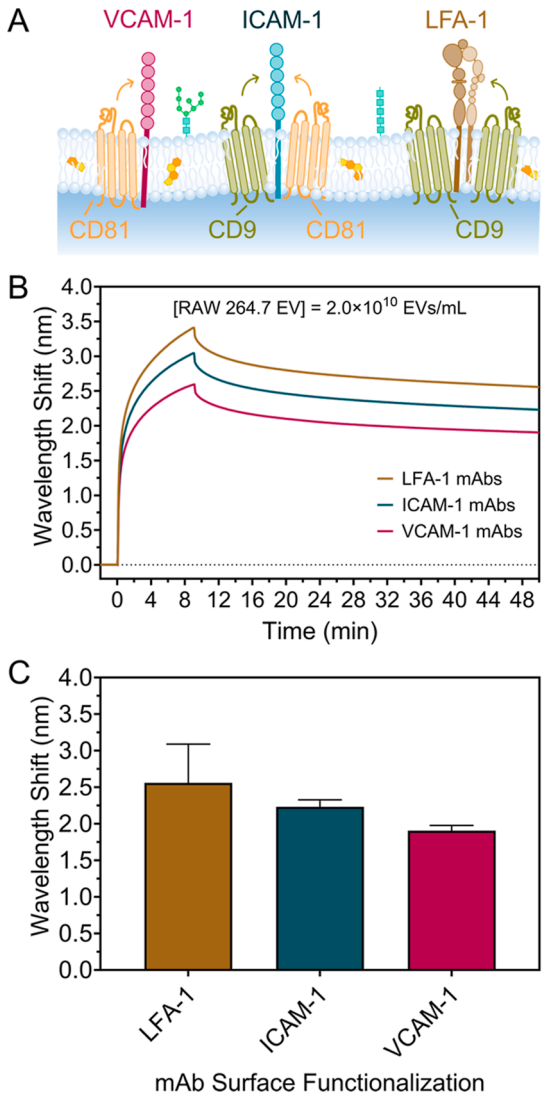

Figure 4. (A) Schematic of the EV surface expressing nontetraspanin TMPs LFA-1, ICAM-1, and VCAM-1 and their association with the partner tetraspanins CD9 and CD81, respectively. (B) Real-time SPR sensorgrams and (C) wavelength shift of RAW 264.7 EV capture at a concentration of 2.0 × 10^{10} EVs/mL with LFA-1, ICAM-1, and VCAM-1 mAbs. The Abs were covalently linked on a 9:1 OEG_4OH/OEG_6COOH mixed SAM at a ∼40% Ab surface coverage.

understanding the associations of nontetraspanin TMPs with their tetraspanins partners is imperative as it can offer an alternative means to indirectly profile elusive clinically relevant markers targeting their partner tetraspanins. The results of EV detection targeting nontetraspanin TMPs suggest that a broader TMP biomarker expression panel could be predicted and experimentally confirmed by correlating their detection using SPR biosensors with the expression of their tetraspanin partners.

Dual-mAb Surface Functionalization for Co-targeted EV Detection. To date, most SPR biosensing assays developed for EV detection have targeted individual tetraspanins and TMPs. Limited attention has been given to the formation of TEMs and their impact on EV detection. Studies reveal that besides the primary interactions between tetraspanin−nontetraspanin TMPs in TEMs, secondary interactions in TEMs are weaker and occur between different tetraspanins, leading to the formation of larger clusters of approximately 100 nm in size by linking primary complexes.[68] Therefore, targeting multiple tetraspanins within the TEMs can lead to enhanced EV capture. We investigated EV detection using SPR biosensors with a novel dual-mAb functionalization strategy targeting the universal CD81, CD63, and CD9 tetraspanins, accounting for the formation of TEMs. We used CD81/CD63, CD81/CD9, and CD63/CD9 mAb combinations at feed ratios of 1:3, 1:1, 3:1 to functionalize the SPR biosensor surfaces and co-target tetraspanins on the EV surface (Figure 5A). Figure 5B−D show the SPR sensorgrams for the EV detection on dual-mAb surfaces and the single-mAb surfaces. The SRP sensorgrams with CD81/CD63 dual-mAbs (dotted lines) in Figure 5B show almost identical association curves as those with CD81 and CD63 single-mAbs (solid lines), but less EV dissociation from the dual-mAb surfaces, implying a stronger EV capture by the CD81/CD63 dual-mAb surfaces compared to the CD63 and CD81 single-mAb surfaces. Similar trends are observed for other dual-mAb and individual mAb functionalized surfaces in Figure 5C,D. These results indicate that the dual-mAb surfaces tend to reduce the dissociation of EVs captured on the surfaces, which can bind EVs stronger on the sensing surfaces hence, enhancing detection sensitivity.

The wavelength shift statistics for EV capture on the dual-mAb and the corresponding single-mAb surfaces are shown in Figures 5E−G. The black dotted lines in these figures represent the predicted linear relationships for EV capture based on individual mAbs without considering the effects of co-targeting, which means CD63 and CD81 mAbs binding two different EVs *via* CD63 and CD81 tetraspanins, respectively, rather than binding the same EV *via* CD63 and CD81 on TEMs. The wavelength shifts for EVs bound to dual-mAb surfaces were higher than these predicted values. In Figure 5E, CD81/CD63 dual-mAbs at ratios of 1:3 and 3:1 exhibited wavelength shifts of 3.78 ± 0.37 nm and 3.33 ± 0.25 nm, respectively, surpassing the predicted values of 3.19 ± 0.42 nm and 2.68 ± 0.29 nm. The 1:1 CD81/CD63 dual-mAb case showed a wavelength shift of 3.04 ± 0.08 nm, which was close to the predicted value of 2.94 ± 0.32 nm. For the CD81/CD9 dual-mAb surfaces (Figure 5F), the wavelength shifts at ratios of 1:3 and 3:1 were 6.82 ± 0.08 nm and 4.80 ± 0.23 nm, respectively, compared to the predicted values of 6.30 ± 0.74 nm and 3.72 ± 0.35 nm. The 1:1 CD9/CD81 dual-mAb surface had a wavelength shift of 5.08 ± 0.14 nm, which was close to the predicted value of 5.01 ± 0.52 nm. Figure 5G shows consistently higher wavelength shifts for EVs captured with CD63/CD9 dual-mAb surfaces, with values of 7.17 ± 0.39 nm, 6.06 ± 0.27 nm, and 5.08 ± 0.30 nm for ratios of 1:3, 1:1, and 3:1, respectively, compared to the predicted values of 6.55 ± 0.75 nm, 5.51 ± 0.56 nm, and 4.48 ± 0.48 nm. Statistical analysis indicates a significant increase in EV capture for the CD81/CD63 and CD81/CD9 dual-mAb surfaces at the 3:1 ratio, suggesting that the cotargeting effect enhances EV capture efficiency.

To verify the cotargeting effect from dual-mAb surfaces, we profiled the tetraspanins on EVs captured with 1:3, 1:1, and 3:1 CD81/CD63 dual-mAb surfaces using a sandwich assay as depicted in Figure S6A. The responses from the sandwich CD9, CD63 and CD81 mAbs on EVs captured by the 1:1 CD81/CD63 dual-mAb surface are lower than those on the EVs captured by the 1:3 and 3:1 CD81/CD63 dual-mAb surfaces (Figure S6B). These observations correlate with the amount of EVs captured on the dual-mAb surfaces. Notably,

https://doi.org/10.1021/acs.analchem.4c04086
Anal. Chem. 2024, 96, 16406−16414

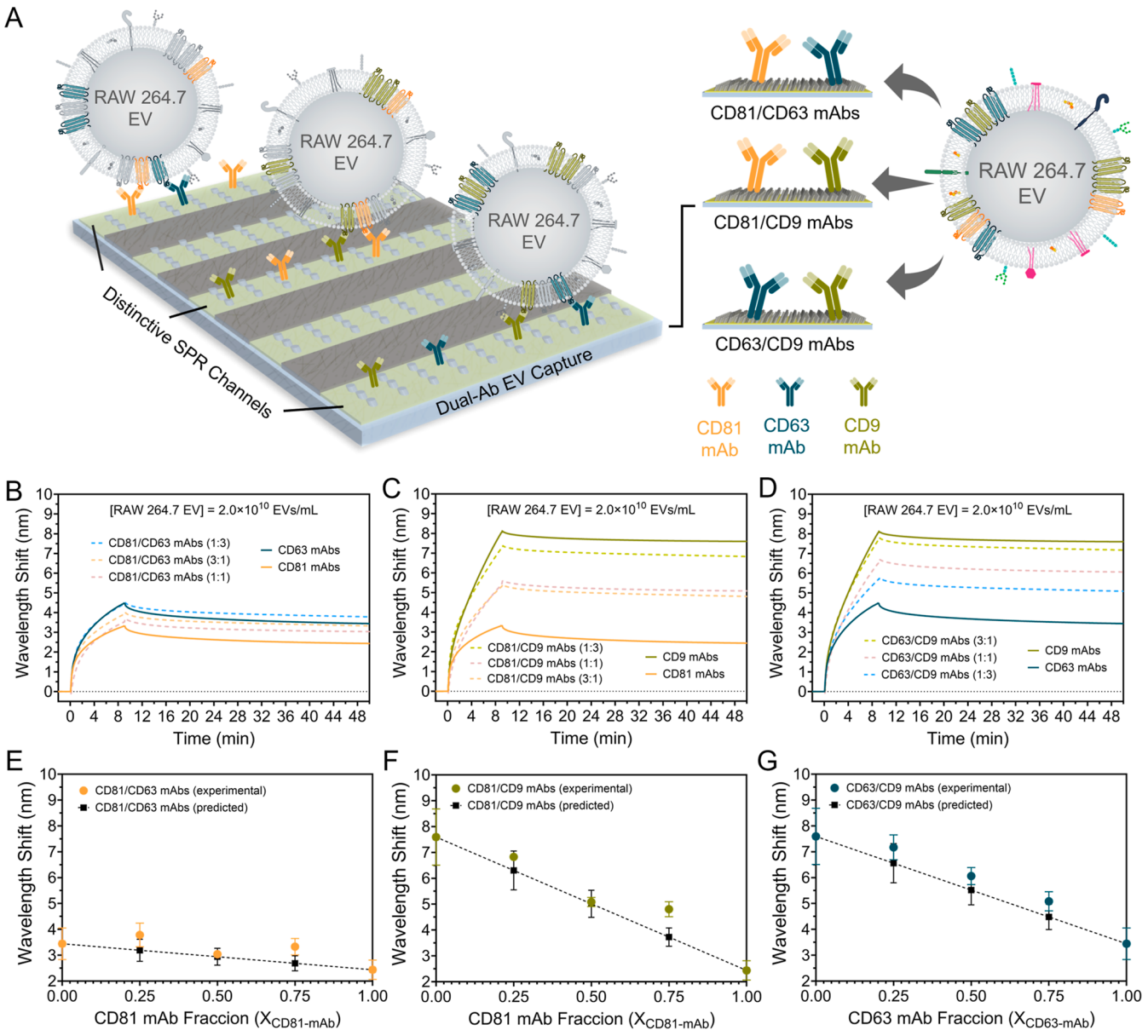

Figure 5. (A) Schematic representation of RAW 264.7 EV detection using a dual-mAb approach. (B–D) Real-time SPR sensorgrams of RAW 264.7 EV capture at a concentration of 2.0×10^{10} EVs/mL with CD81/CD63, CD81/CD9, CD63/CD9 dual-mAbs at ratios of 1:3, 1:1, and 3:1, respectively (dotted curve), with individual CD81, CD63, and CD9 mAbs (solid curve). (E–G) Wavelength shift of RAW 264.7 EV capture as a function of the ratio of dual-mAbs plotted with the corresponding results in (B–D). The black dotted lines are the linear relationships between two single-mAbs.

CD9 mAb sandwich responses are dramatically higher compared to CD63 and CD81 mAb responses, which may be due to the high expression level of CD9 tetraspanin on EVs or the possibility that CD9 tetraspanin does not form TEMs with CD63 and CD81 tetraspanins. Interestingly, for each dual-mAb ratio, the CD63 mAb sandwich wavelength shifts were lower than the CD81 mAb, contradicting our previous observations with EVs captured *via* single-mAb functionalized surfaces. This suggests that in dual-mAb surfaces, the enhanced EV capture is a consequence of cotargeting CD63 and CD81 tetraspanins, with a higher binding efficiency to CD63 tetraspanin than CD81 tetraspanin. Consequently, more CD63 tetraspanins are occupied during EV capture, reducing their availability for binding during the sandwich assay. To investigate whether more CD81 tetraspanins remain unoccupied on captured EVs, we performed a sandwich assay using a CD81 mAb concentration of 80 μg/mL, which is four times higher than the previous concentration of 20 μg/mL. This assay was performed with EVs captured using the same CD81/CD63 dual-mAb surfaces ratios (Figure S7). Unlike the sensorgrams from a lower sandwich CD81 mAb concentration of 20 μg/mL (Figure S6E), which exhibited plateaus, the SPR wavelength shifts for the higher sandwich CD81 mAb concentration of 80 μg/mL increased over time without reaching a plateau, resulting in a larger wavelength shift (~0.8 nm *vs* ~0.1 nm). This indicates that more CD81 tetraspanins are unoccupied during EV capture. Similar trends are anticipated if mAb concentrations are increased in sandwich assays targeting CD9 and CD63 tetraspanins, which could be advantageous for signal amplification in EV marker profiling.

https://doi.org/10.1021/acs.analchem.4c04086
Anal. Chem. 2024, 96, 16406−16414

The cotargeting effect could enhance detection sensitivity. We evaluated this by using dual-mAb surfaces to push the limit of detection (LOD) for EVs captured with CD9 mAbs, given that CD9 mAbs show the highest EV capture efficiency among three single-mAb surfaces tested. The LOD and linear range of the SPR biosensor as well as the EV binding kinetics using CD9-mAb functionalized surfaces are detailed in Figures S8−10 and described in the Supporting Information. The estimated LOD was 2.6×10^5 EVs/mL using the SPR biosensor, and it was 1.5×10^7 EVs/mL with ELISA (Figure S11). To challenge this LOD, we used CD9/CD81 dual-mAb surfaces at 4:1 and 9:1 ratios to detect EVs at a concentration of 2.0×10^5 EVs/mL. As illustrated in Figure 6, there were no

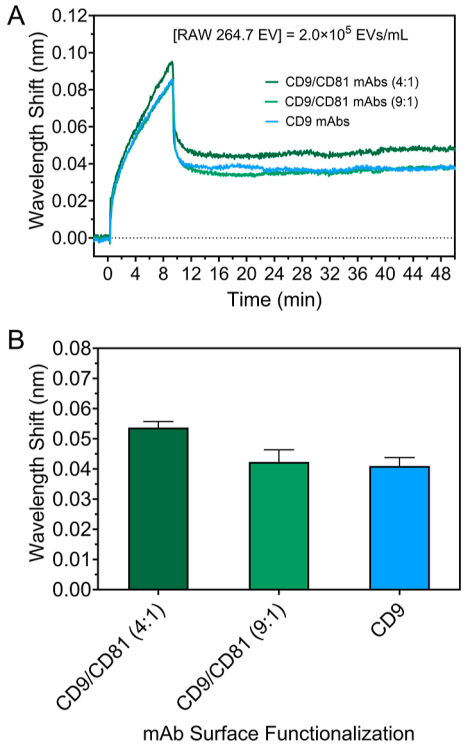

Figure 6. (A) Real-time SPR sensorgrams and (B) wavelength shift of RAW 264.7 EV capture at a concentration of 2.0×10^5 EVs/mL with CD9/CD81 dual-mAbs at ratios of 4:1 and 9:1 and CD9 single-mAbs.

detectable wavelength shift differences between EVs captured with the CD9 single-mAb surface and the 9:1 CD9/CD81 dual-mAb surface. However, the 4:1 CD9/CD81 dual-mAb surface exhibited a statistically significant enhancement in EV detection (p value < 0.05), improving the LOD. These findings suggest that dual-mAb surface functionalization can effectively improve the LOD for EV detection and capture efficiency. Additionally, sandwich assays can be used to further profile and detect biomarkers on captured EVs. Combining these strategies offers a powerful approach for detecting and profiling clinically relevant EVs using SPR biosensors in medical diagnostics.

CONCLUSIONS

In this study, we developed a series of SPR biosensor immunoassays based on dual-mAb functionalization to co-target tetraspanins on the surface of EVs derived from a leukemic mouse cell line. We identified the expression levels of tetraspanin markers on RAW 264.7 derived EVs revealing a trend of CD9 > CD63 > CD81 from the SPR-based sandwich immunoassay and ELISA measurements. When targeting nontetraspanin TMPs, we observed a trend of LFA-1 > ICAM-1 > VCAM-1, consistent with the expression levels of their primary tetraspanin partners, CD9 and CD81, respectively. The dual-mAb functionalization strategy demonstrated enhanced EV capture, due to cotargeting tetraspanins. This approach offers a promising method for significantly improving EV capture and indirectly profiling clinically relevant non-tetraspanin TMPs by targeting their associated tetraspanin partners. The surface chemistry proposed in this work is suitable for EV samples isolated and stored in buffer. Further exploration into highly specific and low fouling chemistries that will enable detection of undiluted EVs from serum is needed for the application of dual-mAb surfaces to clinical samples.

ASSOCIATED CONTENT

Supporting Information

The Supporting Information is available free of charge at https://pubs.acs.org/doi/10.1021/acs.analchem.4c04086.

Chemical reagents; Experimental details on the EV Immunocapture using ELISA; NTA graphs showing size distributions for RAW 264.7 EV batches used; SPR sensorgrams and wavelength shifts for replicates of EVs detected with CD81, CD63, and CD9 mAbs; SPR sensorgrams and wavelength shifts for replicates of EVs detected CD9 mAbs at varying concentrations; non-linear global fitting for association and dissociation phases of EVs captured with CD9 mAbs; SPR sensorgrams of sandwich assay with CD81, CD63, and CD9 mAbs post EV capture with CD9 mAbs; SPR sensorgrams of sandwich assay with CD81, CD63, and CD9 mAbs post EV capture with CD81/CD63 dual-mAbs surfaces; SPR sensorgrams and wavelength shift of SPR-based sandwich assay with high concentration of CD81 mAbs; percent homology of the conserved region of the EC2 loop of CD81, CD63, and CD9 tetraspanins (PDF)

AUTHOR INFORMATION

Corresponding Author

Qiuming Yu − *Robert Frederick Smith School of Chemical and Biomolecular Engineering, Cornell University, Ithaca, New York 14853, United States;* orcid.org/0000-0002-2401-4664; Email: qy10@cornell.edu

Authors

Jesus M. Lopez Baltazar − *Robert Frederick Smith School of Chemical and Biomolecular Engineering, Cornell University, Ithaca, New York 14853, United States;* orcid.org/0009-0004-7704-093X

Wenchao Gu − *Meinig School of Biomedical Engineering, Cornell University, Ithaca, New York 14853, United States;* orcid.org/0000-0002-0967-1682

Complete contact information is available at: https://pubs.acs.org/10.1021/acs.analchem.4c04086

Notes

The authors declare no competing financial interest.

https://doi.org/10.1021/acs.analchem.4c04086
Anal. Chem. 2024, 96, 16406−16414

■ ACKNOWLEDGMENTS

The authors gratefully acknowledge the financial support by the National Science Foundation (NSF) (CBET-2247222). J.M.L.B. acknowledges the support from the National GEM Consortium Fellowship. This work was performed in part at the Cornell NanoScale Facility, a member of the National Nanotechnology Coordinated Infrastructure (NNCI), which is supported by the NSF (grant NNCI-2025233). Any opinion, findings, and conclusions or recommendations expressed in this material are those of the authors and do not necessarily reflect the views of the NSF.

■ REFERENCES

(1) Rakshit, T.; Pal, S. *JACS Au* **2024**, *4* (2), 318−327.
(2) Bari, S. M. I.; Hossain, F. B.; Nestorova, G. G. *Sensors* **2021**, *21* (22), 7645.
(3) Carnino, J. M.; Lee, H.; Jin, Y. *Respir. Res.* **2019**, *20* (1), 240.
(4) Cheng, S.; Li, Y.; Yan, H.; Wen, Y.; Zhou, X.; Friedman, L.; Zeng, Y. *Lab Chip* **2021**, *21* (17), 3219−3243.
(5) Cloet, T.; Momenbeitollahi, N.; Li, H. *Anal. Biochem.* **2021**, *622*, 114168.
(6) Li, G.; Tang, W.; Yang, F. *Biotechnol. J.* **2020**, *15* (5), No. e1900225.
(7) Risha, Y.; Minic, Z.; Ghobadloo, S. M.; Berezovski, M. V. *Sci. Rep.* **2020**, *10* (1), 13572.
(8) Vitale, S. R.; Helmijr, J. A.; Gerritsen, M.; Coban, H.; van Dessel, L. F.; Beije, N.; van der Vlugt-Daane, M.; Vigneri, P.; Sieuwerts, A. M.; Dits, N.; et al. *BMC Cancer* **2021**, *21* (1), 315.
(9) Wang, W.; Luo, J.; Wang, S. *Adv. Healthcare Mater.* **2018**, *7* (20), No. e1800484.
(10) Armstrong, J. P. K.; Holme, M. N.; Stevens, M. M. *ACS Nano* **2017**, *11* (1), 69−83.
(11) Othman, N.; Jamal, R.; Abu, N. *Front. Immunol.* **2019**, *10*, 2103.
(12) van der Pol, E.; Böing, A. N.; Harrison, P.; Sturk, A.; Nieuwland, R. *Pharmacol. Rev.* **2012**, *64* (3), 676−705.
(13) Raposo, G.; Nijman, H. W.; Stoorvogel, W.; Liejendekker, R.; Harding, C. V.; Melief, C. J.; Geuze, H. J. *J. Exp. Med.* **1996**, *183* (3), 1161−1172.
(14) Fais, S.; O'Driscoll, L.; Borras, F. E.; Buzas, E.; Camussi, G.; Cappello, F.; Carvalho, J.; Cordeiro da Silva, A.; Del Portillo, H.; El Andaloussi, S.; et al. *ACS Nano* **2016**, *10* (4), 3886−3899.
(15) Tenchov, R.; Sasso, J. M.; Wang, X.; Liaw, W.-S.; Chen, C.-A.; Zhou, Q. A. *ACS Nano* **2022**, *16* (11), 17802−17846.
(16) Hassanpour Tamrin, S.; Sanati Nezhad, A.; Sen, A. *ACS Nano* **2021**, *15* (11), 17047−17079.
(17) Ibsen, S. D.; Wright, J.; Lewis, J. M.; Kim, S.; Ko, S.-Y.; Ong, J.; Manouchehri, S.; Vyas, A.; Akers, J.; Chen, C. C.; et al. *ACS Nano* **2017**, *11* (7), 6641−6651.
(18) Richardson, J. J.; Ejima, H. *Chem. Mater.* **2019**, *31* (7), 2191−2201.
(19) Ko, J.; Wang, Y.; Sheng, K.; Weitz, D. A.; Weissleder, R. *ACS Nano* **2021**, *15* (3), 5631−5638.
(20) Zhong, Y.; Li, H.; Li, P.; Chen, Y.; Zhang, M.; Yuan, Z.; Zhang, Y.; Xu, Z.; Luo, G.; Fang, Y.; et al. *Front. Oncol.* **2021**, *11*, 743556.
(21) Wu, T.; Liu, Y.; Ali, N. M.; Zhang, B.; Cui, X. *ACS Omega* **2023**, *8* (6), 5157−5168.
(22) Zhou, Z.; Yang, Z.; Zhou, L.; Yang, M.; He, S. *Cell Biosci.* **2023**, *13* (1), 59.
(23) Balise, V. D.; Saito-Reis, C. A.; Gillette, J. M. *Front. Cell Dev. Biol.* **2020**, *8*, 598.
(24) Mustonen, A.-M.; Palviainen, M.; Säisänen, L.; Karttunen, L.; Tollis, S.; Esrafilian, A.; Reijonen, J.; Julkunen, P.; Siljander, P. R. M.; Kröger, H.; et al. *Arthritis Res. Ther.* **2024**, *26* (1), 33.
(25) Andreu, Z.; Yáñez-Mó, M. *Front. Immunol.* **2014**, *5*, 442.
(26) Mordica, W. J.; Woods, K. M.; Clem, R. J.; Passarelli, A. L.; Chapes, S. K. *In Vitro Cell. Dev. Biol. Anim.* **2009**, *45* (5−6), 213−225.
(27) Takeda, Y.; Tachibana, I.; Miyado, K.; Kobayashi, M.; Miyazaki, T.; Funakoshi, T.; Kimura, H.; Yamane, H.; Saito, Y.; Goto, H.; et al. *J. Cell Biol.* **2003**, *161* (5), 945−956.
(28) Liu, A.; Jin, S.; Fu, C.; Cui, S.; Zhang, T.; Zhu, L.; Wang, Y.; Shen, S. G. F.; Jiang, N.; Liu, Y. *Int. J. Oral Sci.* **2020**, *12* (1), 33.
(29) Hemler, M. E. *Nat. Rev. Mol. Cell Biol.* **2005**, *6* (10), 801−811.
(30) Yáñez-Mó, M.; Barreiro, O.; Gordon-Alonso, M.; Sala-Valdés, M.; Sánchez-Madrid, F. *Trends Cell Biol.* **2009**, *19* (9), 434−446.
(31) Levy, S.; Shoham, T. *Physiology* **2005**, *20* (4), 218−224.
(32) *Tetraspanins*; Berditchevski, F., Rubinstein, E., Eds.; Springer: Dordrecht, 2013.
(33) Reyes, R.; Monjas, A.; Yánez-Mó, M.; Cardeñes, B.; Morlino, G.; Gilsanz, A.; Machado-Pineda, Y.; Lafuente, E.; Monk, P.; Sánchez-Madrid, F.; et al. *Biochim. Biophys. Acta Mol. Cell Res.* **2015**, *1853* (10), 2464−2480.
(34) Yeung, L.; Hickey, M. J.; Wright, M. D. *Front. Immunol.* **2018**, *9*, Review.
(35) Rohlena, J.; Volger, O. L.; van Buul, J. D.; Hekking, L. H. P.; van Gils, J. M.; Bonta, P. I.; Fontijn, R. D.; Post, J. A.; Hordijk, P. L.; Horrevoets, A. J. G. *Cardiovasc. Res.* **2009**, *81* (1), 187−196.
(36) Boucheix, C.; Rubinstein, E. *Cell. Mol. Life Sci.* **2001**, *58* (9), 1189−1205.
(37) Lim, C. Z. J.; Zhang, L.; Zhang, Y.; Sundah, N. R.; Shao, H. *ACS Sens.* **2020**, *5* (1), 4−12.
(38) Azzouz, A.; Hejji, L.; Kim, K. H.; Kukkar, D.; Souhail, B.; Bhardwaj, N.; Brown, R. J. C.; Zhang, W. *Biosens. Bioelectron.* **2022**, *197*, 113767.
(39) Karimi, N.; Dalirfardouei, R.; Dias, T.; Lötvall, J.; Lässer, C. *J. Extracell. Vesicles* **2022**, *11* (5), No. e12213.
(40) Mathieu, M.; Névo, N.; Jouve, M.; Valenzuela, J. I.; Maurin, M.; Verweij, F. J.; Palmulli, R.; Lankar, D.; Dingli, F.; Loew, D.; et al. *Nat. Commun.* **2021**, *12* (1), 4389.
(41) Mizenko, R. R.; Brostoff, T.; Rojalin, T.; Koster, H. J.; Swindell, H. S.; Leiserowitz, G. S.; Wang, A.; Carney, R. P. *J. Nanobiotechnol.* **2021**, *19* (1), 250.
(42) Chin, L. K.; Son, T.; Hong, J.-S.; Liu, A.-Q.; Skog, J.; Castro, C. M.; Weissleder, R.; Lee, H.; Im, H. *ACS Nano* **2020**, *14* (11), 14528−14548.
(43) Wang, X.; Phan, M. M.; Sun, Y.; Koerber, J. T.; Ho, H.; Chen, Y.; Yang, J. *Anal. Biochem.* **2022**, *646*, 114635.
(44) Kowalczyk, A.; Gajda-Walczak, A.; Ruzycka-Ayoush, M.; Targonska, A.; Mosieniak, G.; Glogowski, M.; Szumera-Cieckiewicz, A.; Prochorec-Sobieszek, M.; Bamburowicz-Klimkowska, M.; Nowicka, A. M.; et al. *Anal. Chem.* **2023**, *95* (25), 9520−9530.
(45) Mazouzi, Y.; Sallem, F.; Farina, F.; Loiseau, A.; Tartaglia, N. R.; Fontaine, M.; Parikh, A.; Salmain, M.; Neri, C.; Boujday, S. *ACS Sens.* **2022**, *7* (6), 1657−1665.
(46) Picciolini, S.; Gualerzi, A.; Vanna, R.; Sguassero, A.; Gramatica, F.; Bedoni, M.; Masserini, M.; Morasso, C. *Anal. Chem.* **2018**, *90* (15), 8873−8880.
(47) Grasso, L.; Wyss, R.; Weidenauer, L.; Thampi, A.; Demurtas, D.; Prudent, M.; Lion, N.; Vogel, H. *Anal. Bioanal. Chem.* **2015**, *407* (18), 5425−5432.
(48) Liu, C.; Zeng, X.; An, Z.; Yang, Y.; Eisenbaum, M.; Gu, X.; Jornet, J. M.; Dy, G. K.; Reid, M. E.; Gan, Q.; et al. *ACS Sens.* **2018**, *3* (8), 1471−1479.
(49) Yang, Y.; Zhai, C.; Zeng, Q.; Khan, A. L.; Yu, H. *Anal. Chem.* **2020**, *92* (7), 4884−4890.
(50) Sina, A. A.; Vaidyanathan, R.; Wuethrich, A.; Carrascosa, L. G.; Trau, M. *Anal. Bioanal. Chem.* **2019**, *411* (7), 1311−1318.
(51) Sina, A. A.; Vaidyanathan, R.; Dey, S.; Carrascosa, L. G.; Shiddiky, M. J.; Trau, M. *Sci. Rep.* **2016**, *6*, 30460.
(52) Deng, Y.; Sun, Z.; Wang, L.; Wang, M.; Yang, J.; Li, G. *Front. Med.* **2022**, *16* (2), 157−175.
(53) Reiner, A. T.; Ferrer, N.-G.; Venugopalan, P.; Lai, R. C.; Lim, S. K.; Dostálek, J. *Analyst* **2017**, *142* (20), 3913−3921.
(54) Homola, J. *Chem. Rev.* **2008**, *108* (2), 462−493.
(55) Homola, J. *Surface Plasmon Resonance Based Biosensors*; Springer, 2006.

(56) Homola, J. *Anal. Bioanal. Chem.* **2003**, *377* (3), 528−539.
(57) Zhang, L.; Gu, C.; Wen, J.; Liu, G.; Liu, H.; Li, L. *Anal. Bioanal. Chem.* **2021**, *413* (1), 83−102.
(58) Liu, C.; Yang, Y.; Wu, Y. *AAPS J.* **2018**, *20* (2), 41.
(59) Lopez Baltazar, J. M.; Gu, W.; Bocková, M.; Yu, Q. *ACS Sens.* **2024**, *9*, 3594−3603.
(60) Vuorio, J.; Škerlová, J.; Fábry, M.; Veverka, V.; Vattulainen, I.; Řezáčová, P.; Martinez-Seara, H. *Sci. Rep.* **2021**, *11* (1), 5239.
(61) Liebhoff, A.-M.; Venkataraman, T.; Morgenlander, W. R.; Na, M.; Kula, T.; Waugh, K.; Morrison, C.; Rewers, M.; Longman, R.; Round, J.; et al. *Nat. Commun.* **2024**, *15* (1), 1577.
(62) Ondruššek, R.; Kvokačková, B.; Kryštofová, K.; Brychtová, S.; Souček, K.; Bouchal, J. *Front. Oncol.* **2023**, *13*, 1140738.
(63) Liang, Y.; Eng, W. S.; Colquhoun, D. R.; Dinglasan, R. R.; Graham, D. R.; Mahal, L. K. *J. Biol. Chem.* **2014**, *289* (47), 32526−32537.
(64) Justo, B. L.; Jasiulionis, M. G. *Int. J. Mol. Sci.* **2021**, *22* (17), 9319.
(65) Warner, R. B.; Najy, A. J.; Jung, Y. S.; Fridman, R.; Kim, S.; Kim, H.-R. C. *Sci. Rep.* **2020**, *10* (1), 2099.
(66) Bailey, R. L.; Herbert, J. M.; Khan, K.; Heath, V. L.; Bicknell, R.; Tomlinson, M. G. *Biochem. Soc. Trans.* **2011**, *39* (6), 1667−1673.
(67) Susa, K. J.; Kruse, A. C.; Blacklow, S. C. *Trends Cell Biol.* **2024**, *34*, 509−522.
(68) Lang, T.; Hochheimer, N. *Curr. Biol.* **2020**, *30* (5), R204−R206.

https://doi.org/10.1021/acs.analchem.4c04086
Anal. Chem. 2024, 96, 16406−16414